Rational design of a eutectic Ni-Al-Ti alloy composited with B2 and $L1_2$ intermetallics for elevated-temperature application

Gao, Mengqi; Wen, Donghui; Huang, Zhaowen; Kong, Fengyu; Liu, Junhu; Li, Qiang; Zhang, Cong; Liu, Chain-Tsuan; Wang, Anding

Published in:
Materials and Design

Published: 01/01/2025

Document Version:
Final Published version, also known as Publisher's PDF, Publisher's Final version or Version of Record

Published version (DOI):
10.1016/j.matdes.2024.113532

Publication details:
Gao, M., Wen, D., Huang, Z., Kong, F., Liu, J., Li, Q., Zhang, C., Liu, C.-T., & Wang, A. (2025). Rational design of a eutectic Ni-Al-Ti alloy composited with B2 and $L1_2$ intermetallics for elevated-temperature application. *Materials and Design*, *249*, Article 113532. https://doi.org/10.1016/j.matdes.2024.113532

Materials & Design 249 (2025) 113532

Contents lists available at ScienceDirect

Materials & Design

journal homepage: www.elsevier.com/locate/matdes

Rational design of a eutectic Ni-Al-Ti alloy composited with B2 and $L1_2$ intermetallics for elevated-temperature application

Mengqi Gao [a,b], Donghui Wen [b,*], Zhaowen Huang [b], Fengyu Kong [b], Junhu Liu [b], Qiang Li [a,c,*], Cong Zhang [d,e], Chain-Tsuan Liu [f], Anding Wang [b,*]

[a] Xinjiang Key Laboratory of Solid State Physics and Devices & School of Physical Science and Technology, Xinjiang University, Ürümqi 830046, Xinjiang, China
[b] Research Institute of Interdisciplinary Science & School of Materials Science and Engineering, Dongguan University of Technology, Dongguan 523808, Guangdong, China
[c] School of Materials Science and Engineering, Xinjiang University, Ürümqi 830046, Xinjiang, China
[d] Institute of High Energy Physics, Chinese Academy of Sciences, Beijing 100049, China
[e] Spallation Neutron Source Science Center, Dongguan 523803, China
[f] Hong Kong Institute for Advanced Study, City University of Hong Kong, China

ARTICLE INFO

Keywords:
Eutectic alloy
Composite structure
Strength
Deformation
High temperature

ABSTRACT

Intermetallic alloys with ordered superlattice phases, e.g., B2-NiAl and $L1_2$-Ni_3Al phases, possess unparalleled strength and structural stability at elevated temperatures, therefore are widely applied in aerospace and energy fields. Improving their castability and room-temperature brittleness is therefore of great significance. In this proof-of-concept study, Ni-Al-Ti alloys with B2 and $L1_2$ intermetallic phases were designed with the help of phase diagram calculation assists composition adjustment. The representative Ni-22Al-7Ti eutectic alloy with a dual-phase lamellar microstructure possesses an ultra-high fracture strength of 3500 MPa and an admirable fracture strain of 30 % under compression at room-temperature. It also possesses a super-high strength of 1180 MPa at 700 °C, overperforming their single-phase counterparts. The superior mechanical property can be attributed to the synergetic deformation of the eutectic structure, R characterization (abnormal yield effect) and the Ti alloying enhanced phase stability at elevated temperatures. The non-equilibrium solidification induced supersaturation also results in the super-high strength at room-to-medium temperature and a unique softening mechanism via the formation of the two-fold composite structure. These results provide a promising candidate alloy for elevated-temperature applications, and a new paradigm for dual-intermetallic eutectic alloy design.

1. Introduction

Improving the service temperature of materials is of great importance for the lightweight, energy efficiency, longevity, and safety of high-temperature (HT) devices used in critical fields like aerospace, nuclear power and etc. [1,2]. Among the large family of HT materials, Ni-Al-based alloys, especially those containing ordered intermetallic B2-NiAl and $L1_2$-Ni_3Al phases [3–5], have attracted great attention because of the exceptional mechanical properties and microstructural stability at HT compared with traditional disordered alloys. The superior performance of intermetallic alloys can be attributed to the stable long-range ordered crystalline structures even up to their melting points and the coexistence of metallic and covalent bonds [6,7]. Hence, the strong binding and close packing among all components of intermetallic alloys endow super-high softening resistance and have attracted significant interest among the material community [8,9].

After extensive studies, the corresponding mechanic properties, deformation behaviors, strengthening and phase formation mechanisms of Ni-Al-based alloys have been well extensively investigated, including single and multi-phases solid solution and intermetallic alloys [10–13]. To be clarity, the face-centered and body-centered cubic structured single solution phases are labeled as face-centered cubic (FCC) and body-centered cubic (BCC), and this study mainly focuses on the FCC and BCC typed intermetallic phases, which are labeled as $L1_2$ and B2. As shown in Fig. 1, the B2-NiAl and $L1_2$-Ni_3Al single-phase intermetallic alloys generally exhibit superior HT strength and thermal stability,

* Corresponding authors at: Xinjiang Key Laboratory of Solid State Physics and Devices & School of Physical Science and Technology, Xinjiang University, Ürümqi 830046, Xinjiang, China (Qiang Li).
E-mail addresses: dhwen@dgut.edu.cn (D. Wen), qli@xju.edu.cn (Q. Li), anding.w@dgut.edu.cn (A. Wang).

https://doi.org/10.1016/j.matdes.2024.113532
Received 8 October 2024; Received in revised form 7 December 2024; Accepted 9 December 2024
Available online 12 December 2024

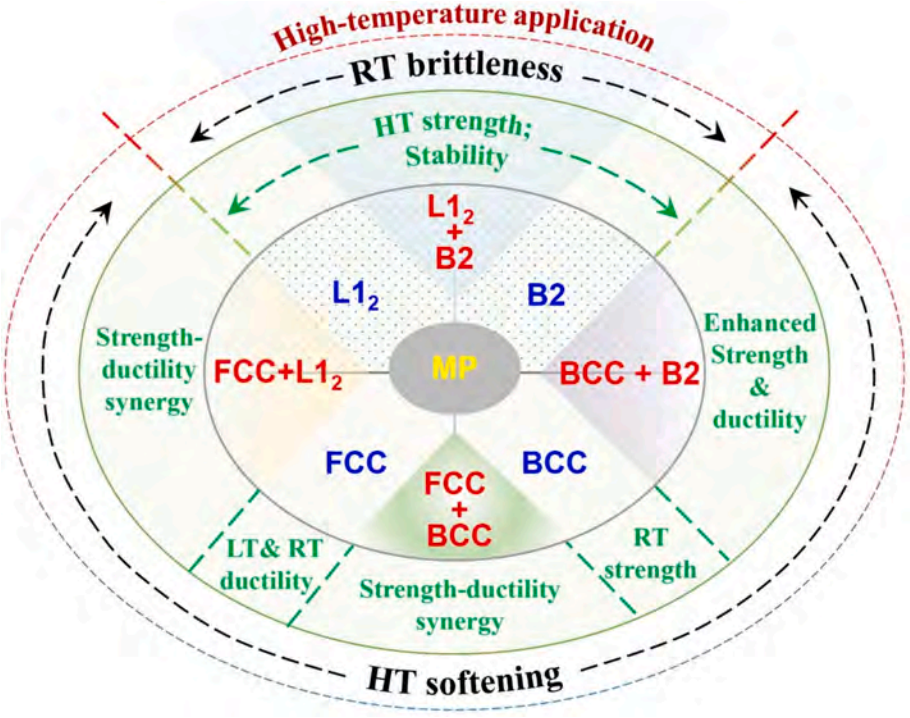

Fig. 1. Typical phase structure of Ni-Al-based alloys and their multicomponent derivatives, including single-phase (blue), dual-phase (red), and multiple-phase (MP, in yellow color), as well as their advantages (green) and shortcomings (black).

owing to the yield strength (YS) increases with increasing temperature (which is called R characterization) [14,15]. However, the single-phase intermetallic alloy is commonly characterized by room temperature (RT) brittleness due to the insufficient slip system and poor grain boundary cohesion, which seriously limits their practical usability [16]. The single-phase solid solution alloys with FCC and BCC structures developed via a multi-component strategy exhibit unique low temperature and RT ductility and exceptional RT strength [17–19], respectively. Nevertheless, most single-phase FCC multi-component alloys possess low YS (only around 200 MPa) at HT, which limits their engineering applications in many cases [20]. In order to restrain the brittleness of single-phase intermetallic alloys and enhance the HT softening resistance of single-phase solid solution alloys, numerous dual-phase and multi-phase alloys with composite structures [21–23] are developed to combine the strength and ductility by instilling synergistic deformation mechanism [24]. It has been found that the FCC and BCC dual-phases can balance strength and ductility [25,26]. Moreover, introducing second intermetallic phase has been demonstrated as an effective approach to impede dislocation motions and in turn strengthen the alloy accordingly [27,28]. In most Ni-Al-based superalloys, the FCC matrix can be strengthened by the $L1_2$ precipitation [29,30]. In BCC-based alloys, the spherical or cuboidal B2 nanoparticles coherently precipitate in the matrix by adjusting the lattice mismatch between BCC and B2 phases, by which the unprecedent strength-ductility synergy could be obtained [31,32]. However, different from the structural materials designed for RT application, the HT alloys require more critical performances [1,2], including thermal stability, ductility, softening resistance, and etc. The softening behavior of solid solution containing alloys is known as a big obstacle for HT applications. It is therefore of great interest to design dual-phase intermetallic alloys with a composite structure.

The composite alloys with B2 and $L1_2$ intermetallics emerged recently, shedding light on overcoming the RT brittleness dilemma without sacrificing the stability [33]. In particular, these alloys closing to the eutectic point can additionally exhibit excellent castability, and further improve the mechanical properties via forming fine eutectic microstructure [34,35]. Such a fine intermetallic composite alloy design strategy has been proved by Shi et al. in a multicomponent alloy [36]. By constructing a special fishbone like eutectic intermetallic alloys with B2 and $L1_2$ phases via a directional solidification technique, extremely high elongation (> 50%) and exceptional comprehensive properties were obtained. These results inspire us to develop new and scalable eutectic intermetallic alloys for common solidification processes, to decrease the materials cost and widen the application prospect, which is still challenging as we know. In addition, the cooling rate determined non-equilibrium solidification could have strong influences on the precipitation behavior and microstructure of the dual-intermetallic alloys, which should be of great scientific interests. Consequently, it is visionary for us to develop B2 and $L1_2$ composite alloys.

In this study, Ni-Al-Ti system alloys with B2 and $L1_2$ composite structures were designed via the alloy system selection and composition adjustment with the assistance of the phase diagram calculation (CALPHAD), as shown in Fig. 2a. The mechanical property and microstructural stability of the representative Ni-22Al-7Ti (at. %) eutectic alloy were investigated systematically. It is found that our newly designed dual-intermetallic alloy possesses a superior synergy of castability, structural stability, and mechanical properties, as well as a relatively low density. The eutectic intermetallic alloys with a novel hierarchical microstructure of thermally stable B2 and $L1_2$ show great application prospects and can be a new paradigm for the future development of castable materials for HT applications.

2. Alloy design strategies

In order to develop the dual-phase intermetallic eutectic alloys with NiAl (B2) and Ni_3Al ($L1_2$) phases for HT applications, the following strategies and routes in Fig. 2b are used:

1) Alloy system determination: in the Ni-Al binary phase diagram (Fig. 2c) [37], no eutectic point of the B2-NiAl and $L1_2$-Ni_3Al phases can be found. In the Ni-Al-Ti ternary phase diagrams (Fig. 2d), there is a eutectic line of B2 and $L1_2$ in the low Ti content side, indicating

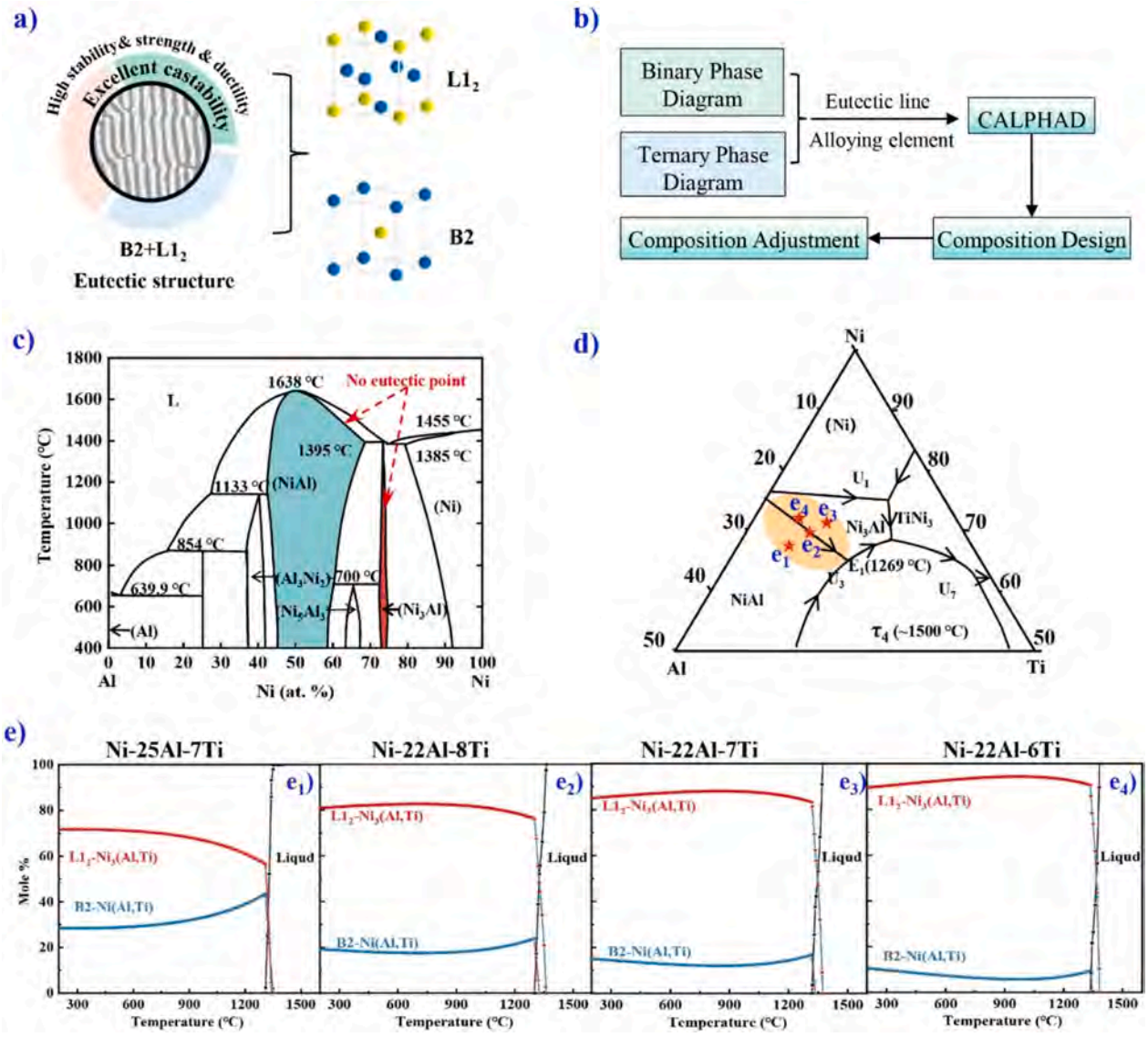

Fig. 2. a) Sketch of the desired composite structure with the B2 and $L1_2$ intermetallics, as well as the desired properties; b) design strategy and investigation route of the eutectic intermetallic alloy; c) Ni-Al binary phase diagram [37], showing the absence of B2 and $L1_2$ dual-phase region; d) Ni-Al-Ti ternary phase diagram [38], showing the eutectic line in stable state and the possible eutectic region enlarged by the non-equilibrium solidification; e) phase diagrams of representative alloys in the eutectic region calculated by using the JmatPro software.

Ti can stabilize the intermetallic [38,39]. It has also been reported that the substitution of Al by Ti will reduce the propensity for environmental embrittlement of Ni-based alloys. Therefore, the Ni-Al-Ti system is selected.

2) Composition selection criteria: since the high solidification rate during casting can enlarge the eutectic composition range, the alloys calculated by using the CALPHAD should be expanded to a certain region as illustrated in Fig. 2d. Phase diagrams of typical Ni-Al-Ti alloys with different phase proportions are calculated by the JmatPro software, and partial results are shown in Fig. 2e. Accordingly, all of the four alloys showing eutectic characters, are selected as the representative alloys for further studies.
3) Experimental verification: representative alloys shown in Fig. 2d were prepared and their solidification microstructure was comparatively examined. According to the microstructure of as-cast alloys, the representative alloy was selected.

3. Experimental procedure

Alloy ingots with nominal compositions (at. %) of Ni-25Al-7Ti, Ni-22Al-8Ti, Ni-22Al-7Ti, Ni-22Al-6Ti, Ni-Al and Ni-25Al were prepared by using the arc melting technique under Ar-atmosphere. The influences of material purity and preparation process is evaded to give a better comparison. All samples were melted five times to ensure composition homogeneity. The four-section (diameter: 3–2.5–2–1.5mm) Ni-22Al-7Ti alloy rods were prepared under the same experimental conditions, for subsequent mechanical tests and microstructure characterizations. The samples were annealed at 800 °C and 1000 °C for 100h followed by air cooling to RT for stability evaluation. The thermal behavior of the as-cast alloy was analyzed by a HT differential scanning calorimeter (DSC, Mettler TGA/DSC3+) under an Ar-atmosphere at heating and cooling rates of 40 K/min and 10 K/min. The density of the alloy was measured by the Archimedean method, and the precision of balance was 0.1 mg. Phases of alloys were identified by utilizing an X-ray diffractometer (XRD, Bruker D8) with a Cu-Kα radiation. The microstructure was analyzed by using the optical microscopy (OM, DMi8) and scanning

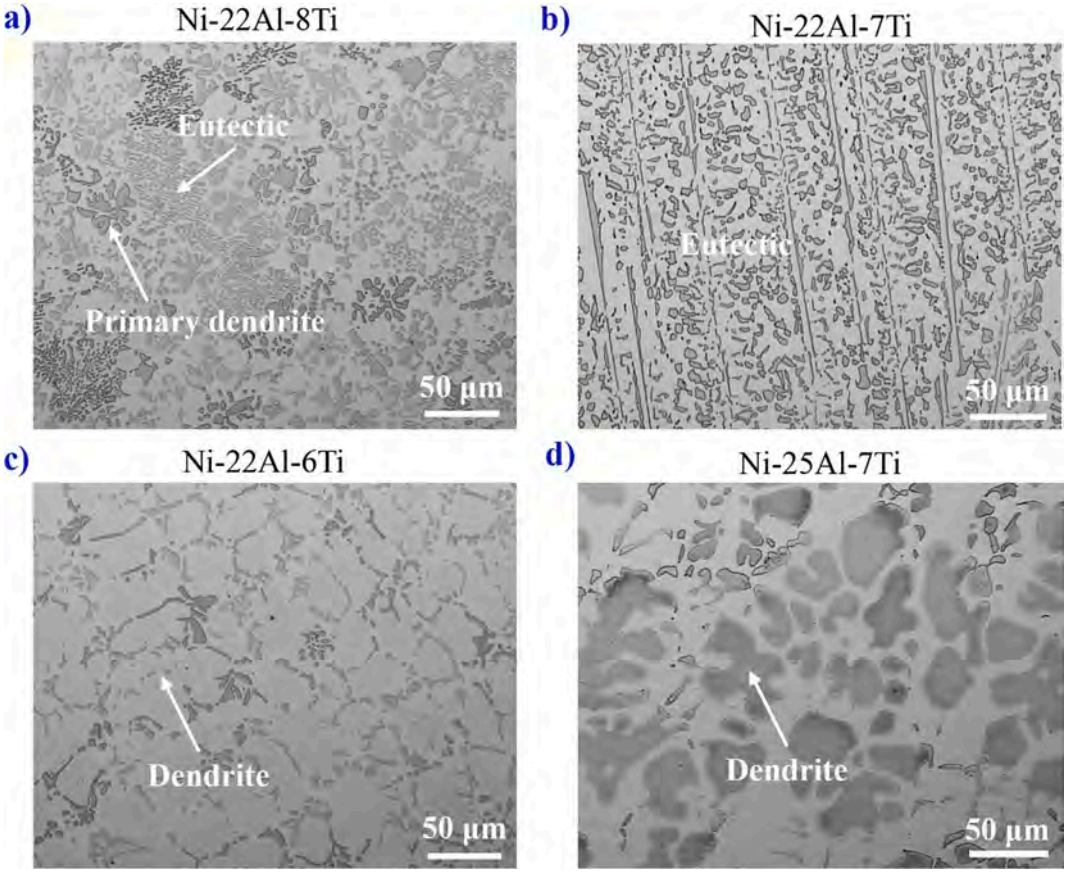

Fig. 3. OM images of typical as-cast Ni-Al-Ti alloy rods, showing the solidification structure of the cross-section.

electron microscope (SEM, JEOL JSM-IT800). Before observation, samples were mechanically polished, and then chemically etched for 10 s with a mixed solution of 20% HF + 10% HNO_3 + 70% H_2O (volume fraction). The crystalline structures of different phases and dislocation distribution were further identified by the transmission electron microscope (TEM, TALOS F200S) coupled with the selected area electron diffraction (SAED) equipment. The phase chemical composition was analyzed by using the energy-dispersive spectrometer (EDS) in SEM and TEM. The Vickers hardness was measured by a hardness tester (Leica Duramin 40 Micro-Hardness), with a load of 500 gf for 15 s. The final standard deviations were determined by averaging more than 10 independent test data on each sample. Compression tests were carried out on the universal mechanical testing machine at RT-1000 °C with commonly used rates of 10^{-4} s^{-1} and 10^{-3} s^{-1} [40]. For the sample soften at HT, the high strain rate is used to shorten the testing time to evading the aging effect. The cylindrical samples with 3 mm in diameter and 6 mm in length, cut from the as-cast ingots for compression show small anisotropy. The strain–stress curves were corrected according to the modulus [3,41–43]. After compression, the cross section of the samples was to identify the deformed microstructures.

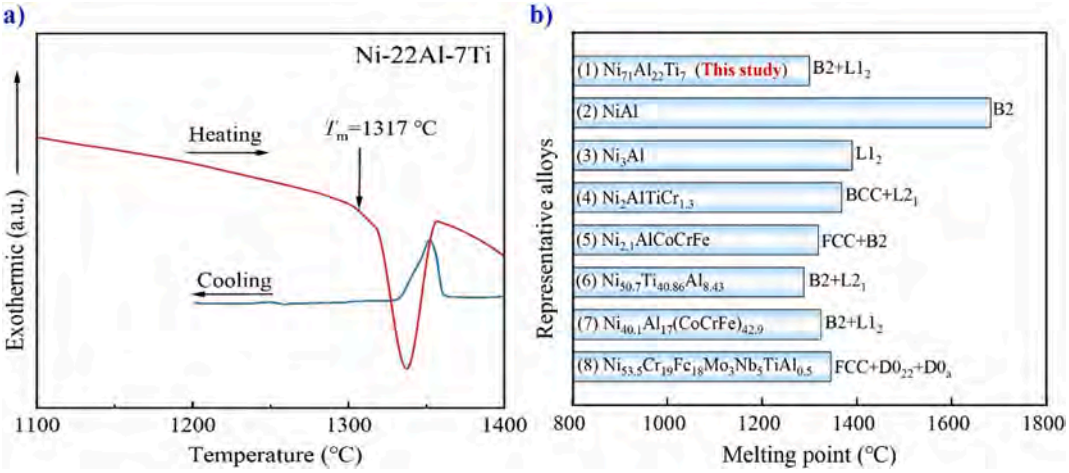

Fig. 4. a) DSC curves of the as-cast Ni-22Al-7Ti alloy measured with heating and cooling rates of 40 K/min and 10 K/min, respectively, showing the melting and solidification behaviors; b) Comparison of melting temperatures (T_m) of representative alloys, i.e. single-phase intermetallic alloys (2,3) [9], intermetallic-solid solution eutectic alloys (4,5) [46,47], dual-phase intermetallic eutectic alloys (6,7) [44,45]and intermetallic precipitated alloys (8) [48].

Table 1
Composition, structure, and melting point of the typical alloys for comparison.

Alloys	Composition	Structure	T_m (°C)	Ref.
1	$Ni_{71}Al_{22}Ti_7$	B2 + $L1_2$ eutectic	1300	This study
2	NiAl	B2 intermetallic	1683	[9]
3	Ni_3Al	$L1_2$ intermetallic	1390	[9]
4	$Ni_2AlTiCr_{1.3}$	BCC + $L2_1$ eutectic	1368	[46]
5	$Ni_{2.1}AlCoCrFe$	FCC + B2 eutectic	1319	[47]
6	$Ni_{50.7}Ti_{40.86}Al_{8.43}$	B2 + $L2_1$ near eutectic	1288	[44]
7	$Ni_{40.1}Al_{17}(CoCrFe)_{42.9}$	B2 + $L1_2$ eutectic	1324	[45]
8	$Ni_{53.5}Cr_{19}Fe_{18}Mo_3Nb_5TiAl_{0.5}$	FCC + $D0_{22}$ + $D0_a$	1346	[48]

4. Results

4.1. Microstructure of as-cast samples and solidification behavior

OM images in Fig. 3a-d show the microstructure of the four designed alloys. It is clear that the alloys exhibit quite distinct solidification microstructure. Ni-22Al-8Ti and Ni-22Al-7Ti alloys exhibit lamella composite structures, indicating the eutectic character (Fig. 3a and b). By comparison, the microstructure of Ni-22Al-7Ti is more uniform, indicating it is closer to the eutectic point. For Ni-22Al-6Ti and Ni-25Al-7Ti alloys (Fig. 3c and d), coarse dendrites were found without typical eutectic structure, which is different from the calculated results in Fig. 1e. Therefore, in the following part, Ni-22Al-7Ti is selected as a representative alloy for the in-depth study of solidification behavior and mechanical properties.

To confirm the phase constitution of the Ni-22Al-7Ti eutectic alloy, DSC tests were conducted and the results are shown in Fig. 4a. Only one endothermic and exothermic peaks are detected in the heating and cooling processes, verifying the fully eutectic nature of the alloy. Compared with typical reference alloys listed in Table 1 and comparatively shown in Fig. 4b, the melting point (T_m) of Ni-22Al-7Ti alloy is much lower than the single-phase NiAl and Ni_3Al intermetallic alloys [9]. The T_m is close to other dual-phase intermetallic eutectic alloys [44,45], intermetallic-solid solution eutectic alloys [46,47] and intermetallic precipitated alloys [48]. It indicates that Ti alloying can obviously decrease the T_m of the single intermetallic phase. These results also exhibit that our Ni-22Al-7Ti eutectic alloy has good castability and can be cast with the common casting process.

Fig. 5a shows the profile of the as-cast Ni-22Al-7Ti alloy rod with different diameters. It is noted that the surface is quite smooth and no obvious shrinkage defects can be observed, further indicating the excellent castability for precision casting. As shown in the XRD pattern in Fig. 5b, the as-cast sample is composed of the B2-Ni (Al, Ti) and $L1_2$-Ni_3 (Al, Ti) phases. In Fig. 5c, it is shown that the lamellar structure distributes uniformly and finely, which is the expected eutectic microstructure. EDS analysis reveals that the black region exhibits a higher Al content, corresponds to the B2 phase, and the gray region with a higher Ni content is the $L1_2$ phase (Fig. 5e). It is therefore concluded that an eutectic alloy composited with B2-Ni (Al, Ti) and $L1_2$-Ni_3 (Al, Ti) phases is readily developed. In addition, the measured density is 6.77 g/cm^3, which is close to the theoretical value of 6.86 g/cm^3, and further indicates that its microstructure is dense.

4.2. Mechanical properties of the as-cast Ni-22Al-7Ti alloy

The compression tests were performed at RT to 1000 °C, and the results are shown in Fig. 6a and b. At RT, the dual-phase intermetallic eutectic Ni-22Al-7Ti alloy exhibits exceptionally high strength up to 3500 MPa, and a large compressive fracture strain of about 30%. It is interesting that the YS of this composite structure exhibits an abnormal increase with increasing temperature, which is known as the R character in Ni_3Al-based single-phase intermetallic alloys [49]. The samples therefore exhibit a super-high YS of about 1200 MPa and good work-hardening ability at 500–700 °C. Even at 800–1000 °C, the samples still exhibit a high strength, showing a strong softening resistance. The compressive plasticity increases greatly with increasing temperatures (≥600 °C), and all samples can be compressed into flat discs without fracture even when the strain is higher than 50 %. Such a large plasticity at HT will enable the thermal plastic shaping for facile processing. As collected in Table 2, it is interesting that this dual-intermetallic composite alloy still exhibits a high σ_{ys} even at 700–1000 °C, enabling a large safety margin against fracture. The high strength and excellent HT ductility therefore endow a good application perspective. The compressive mechanical properties and Vickers hardness of as-cast dual-

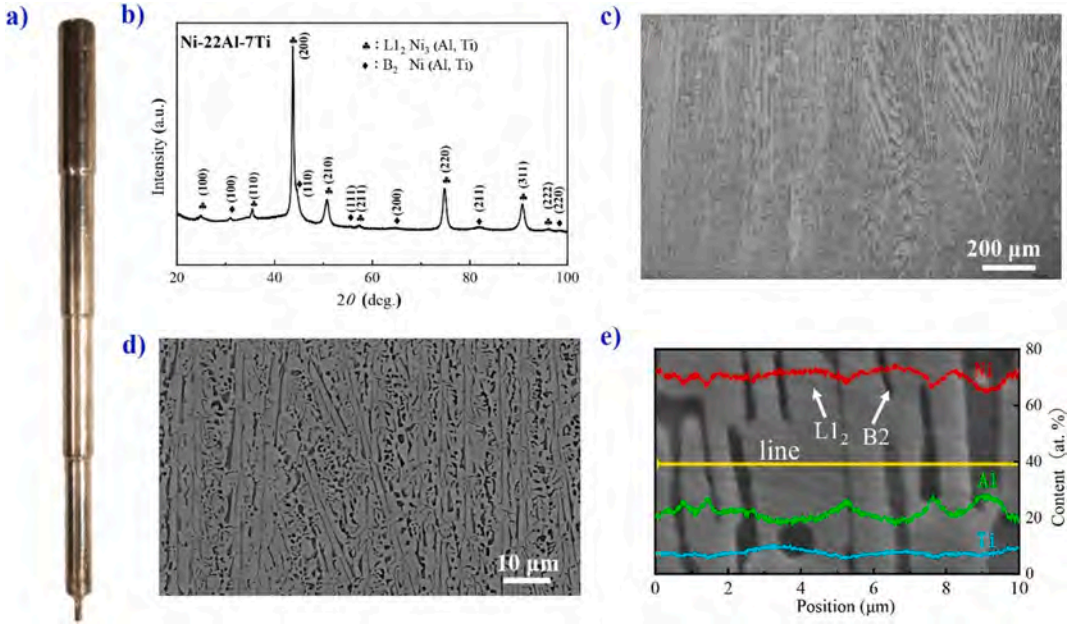

Fig. 5. a) Profile of the four-section rod of the representative Ni-22Al-7Ti alloy; b) XRD pattern; c) OM image shows the eutectic structure; d) SEM image shows the composite structure of the B2 and $L1_2$ phases; e) Line scanning by EDS, showing the composition of the two phases.

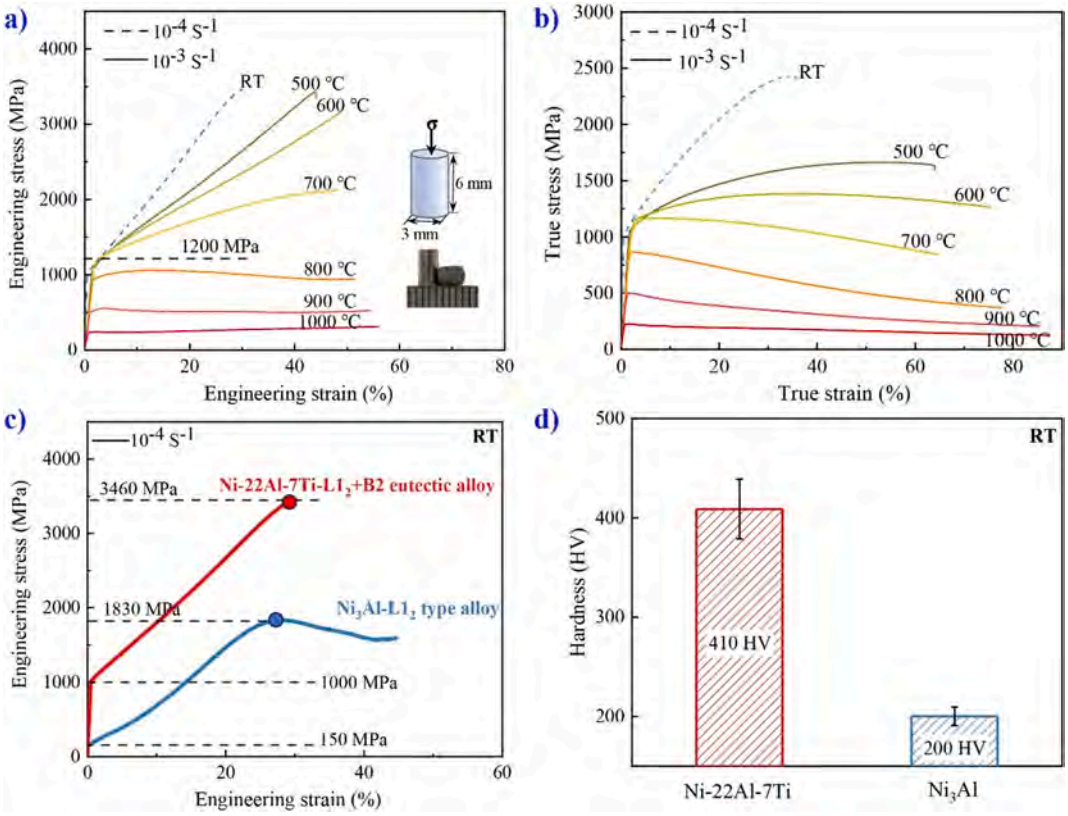

Fig. 6. a) Compressive engineering stress–strain curves of as-cast Ni-22Al-7Ti alloy, the dimension and photo of the sample are inserted; b) The true stress–strain curves transformed from the engineering ones. It is noted that the samples with 50 % strain did not fracture. c) Compressive engineering stress–strain curves of as-cast Ni-22Al-7Ti alloy (B2 + $L1_2$ eutectic) and contrast sample as-cast Ni_3Al ($L1_2$ type) alloy at RT. d) The Vickers hardness of Ni-22Al-7Ti alloy and contrast sample Ni_3Al alloy at RT.

Table 2
Compressive properties of the Ni-22Al-7Ti alloy measured at various temperatures.

Temperature (°C)	Engineering σ_{ys} (MPa)	σ_{ucs} (MPa)	ε (%)	True σ_{ucs} (MPa)	ε (%)
RT	1000	3460	30	2300	35
500	1050	3420	44	1630	65
600	1150	3170	50	1265	75
700	1180	2120	Not	850	65
800	930	940	fracture	370	78
900	500	530		210	85
1000	230	310		125	88

*σ_{ys}: yield strength; σ_{ucs}: ultimate compressive strength; ε: fracture and stopping strains in compression tests.

intermetallic Ni-22Al-7Ti and single-phase Ni_3Al (Ni-25%Al, at. %) alloys prepared with the same process were compared in Fig. 6c and d. It is shown that the σ_{ys} of our designed alloy (1000 MPa) is almost 7 times that of Ni_3Al alloy (150 MPa), the ultimate compressive strength (σ_{ucs}, 3460 MPa) and hardness (410 HV) is 2 times that of Ni_3Al alloy (1830 MPa and 200 HV). With respect to the composite NiAl/Ni_3Al and Ni_3Al alloys, the as-cast NiAl samples are too brittle to be mechanically tested, which indicates that the NiAl/Ni_3Al composite structure and Ti alloying play an important role in improving the comprehensive mechanical performances of the intermetallic alloy.

Fig. 7 comparatively shows the σ_{ys}, σ_{ucs} and ε of the as-cast Ni-22Al-7Ti alloy and typical Al-bearing Ni-based alloys at RT. The Ni-22Al-7Ti sample exhibits excellent comprehensive mechanical properties, including superior synergy of σ_{ys}, σ_{ucs} and ε. Compared with the $Ni_{50.7}Al_{8.43}$-$Ti_{40.86}$ alloy [44] which also has dual-phase intermetallic eutectic structure with B2+$L2_1$, our Ti-lean alloy exhibits lower σ_{ys}, yet larger σ_{ucs} and ε. This should be explained for the following reasons:1) the $L1_2$ phase in our alloy is known to be more ductile than the $L2_1$; 2) the sub-micrometer sized composite structure brings a strong grain-refining strengthening effect; 3) the synergistic deformation process of the B2+$L1_2$ phases will lead to higher work-hardening ability and compressive plasticity. In comparison with the B2+$L1_2$ structured $Ni_{50.7}Al_{19.3}$-$Co_{15}Cr_{15}$ alloy [40], the higher σ_{ucs} should be ascribed to the stronger binding effects among Ti-Ni (ΔH_{mix}: −35 kJ·mol^{-1}) and Ti-Al (ΔH_{mix}: −30 kJ·mol^{-1}) than Co-Ni (ΔH_{mix}: 0 kJ·mol^{-1}) and Cr-Ni (ΔH_{mix}: −7 kJ·mol^{-1}). It is interesting that the mechanic properties of our alloy are even better than intermetallic-solid solution eutectic alloys [31,46,50] and single-phase solid solution alloys with intergranular discontinuous precipitation and brittle phase [51,52]. It is understandable that the obtained mechanic properties are much better than the single-phase intermetallic alloys [53], which originated from the composite structure. From above mechanic property analysis, it can be deduced that the dual-phase intermetallics eutectic alloy design strategy is effective in improving the strength and plasticity of alloys synergistically.

Fig. 8 shows the temperature dependence of the σ_{ys} of the Ni-22Al-7Ti alloy and compared with the typical heat-resistance materials [13,46,54–57]. It is clear that our B2+$L1_2$ composited alloys exhibit the similar σ_{ys} increase–decrease change with the increase of temperature, which is consistent with the R characterization [49]. The σ_{ys} reaches the maximum value of 1180 MPa at about 700 °C. Distinctly, even at 900 °C, it still maintains a high strength of about 500 MPa. Compared with the single-phase intermetallic alloys NiAl [54] and Ni_3Al [13], our alloy exhibits much higher σ_{ys}, which should be attributed to the synergistic deformation of the composite structure. The σ_{ys} of the Ni-22Al-7Ti alloy is much higher than the solid-solution strengthened superalloy (Haynes

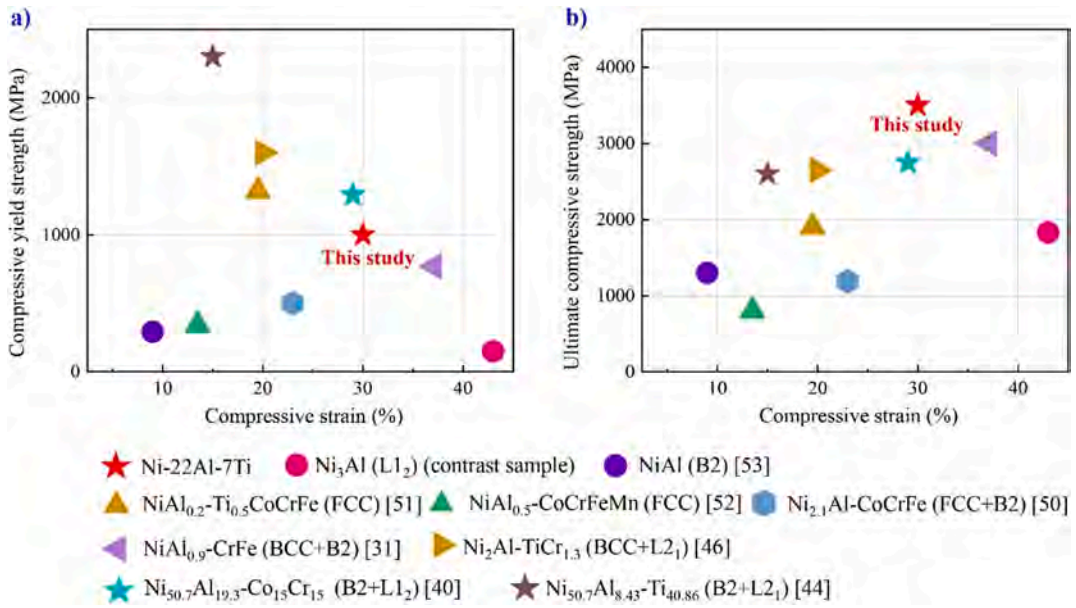

Fig. 7. Yield strength, ultimate compressive strength and strain of the as-cast Ni-22Al-7Ti alloy compressively tested at RT, and other typical reference alloys are also comparatively shown, e.g., the single-phase intermetallic alloys (Ni_3Al and NiAl [53]), the single FCC phase solid solution alloys ($NiAl_{0.2}$-$Ti_{0.5}$CoCrFe [51] and $NiAl_{0.5}$-CoCrFeMn [52]), the intermetallic-FCC solid solution eutectic alloys ($Ni_{2.1}$Al-CoCrFe) [50]and intermetallic-BCC solid solution eutectic alloys ($NiAl_{0.9}$-CrFe [31] and Ni_2Al-$TiCr_{1.3}$ [46]) and the dual-phase intermetallic eutectic alloys ($Ni_{50.7}Al_{19.3}$-$Co_{15}Cr_{15}$) (B2 + $L1_2$) [40] and ($Ni_{50.7}Al_{8.43}$-$Ti_{40.86}$) (B2 + $L2_1$) [44].

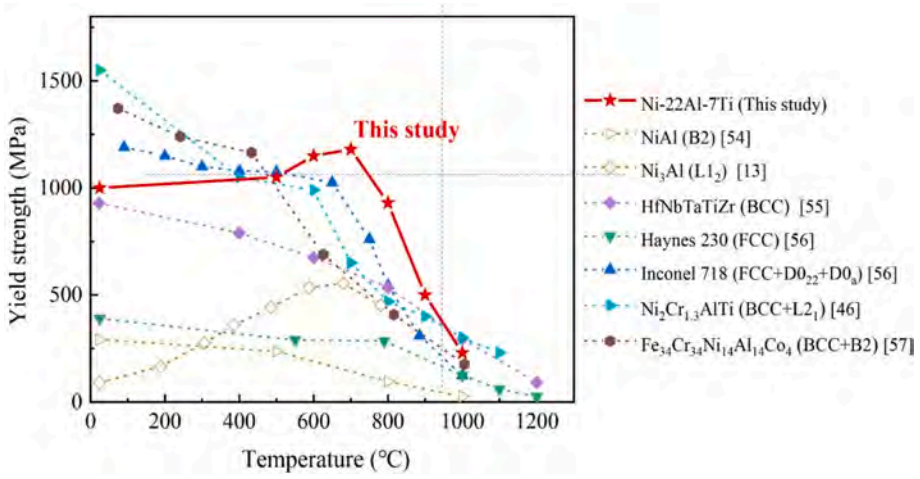

Fig. 8. The temperature dependence of the yield strength of the as-cast Ni-22Al-7Ti alloy and other typical heat-resistance alloys, e.g., the intermetallic alloy (NiAl [54] and Ni_3Al [13]), solid-solution strengthened superalloy (Haynes 230: $Ni_{53}Mo_{16}Cr_{15.5}W_3Fe_3$-$M_{9.5}$) [56], precipitation strengthened superalloy (Inconel 718: $Ni_{53}Cr_{20}Fe_{20}Nb_5Mo_3$-$M_4$) [56], refractory high-entropy alloy (HfNbTaTiZr) [55] and multi-component alloy ($Ni_2Cr_{1.3}AlTi$ [46] and $Fe_{34}Cr_{34}Ni_{14}Al_{14}Co_4$ [57]). All these data are derived from the compressive tests.

230: $Ni_{53}Mo_{16}Cr_{15.5}W_3Fe_3$-$M_{9.5}$) [56]. At 600–900 °C our alloy exhibits the highest σ_{ys}, which is higher than the precipitation strengthened superalloy (Inconel 718: $Ni_{53}Cr_{20}Fe_{20}Nb_5Mo_3$-$M_4$) [56], refractory high-entropy alloys (HfNbTaTiZr) [55] and multi-component alloys ($Ni_2Cr_{1.3}AlTi$ [46] and $Fe_{34}Cr_{34}Ni_{14}Al_{14}Co_4$ [57]). Therefore, the Ni-22Al-7Ti alloy should be a promising candidate for elevated-temperature applications.

4.3. Thermal stability and processability

The safety and advancement of modern elevated-temperature materials not only require mechanical properties, but also rely on phase stability. As shown in Fig. 9, the dual-phase composite structure has good thermal stability. After heat treatment at 800 and 1000 °C for 100h, the samples still exhibit dual-phase composite structure with slight grain coarsening, which is attributed to the mutual inhibition of growth by the dual-phase composite structures. It is important that the B2 and $L1_2$ dual-eutectic structure remains stable even when the temperature reaches 1000 °C, which should be ascribed to the intrinsic stability of these two intermetallics. It should be noted that in the 800 °C treated sample, there are fine precipitates in the B2 phase, which is not consistent with the phase diagram in Fig. 2. The structure evolution mechanism will be discussed in the following part. According to the Fig. 6 and Fig. 9, the designed Ni-22Al-7Ti alloy can maintain dual-phase structure and experience large deformation without fracture at 600–1000 °C, it is therefore deduced that such a composite can exhibit good thermal processability for thermal shaping.

Fig. 10 shows the cross-section morphologies of compressed samples with a strain of 50 %. It is clear that the alloy keeps the uniform composite structure and no crack is found, indicating that the B2 and $L1_2$

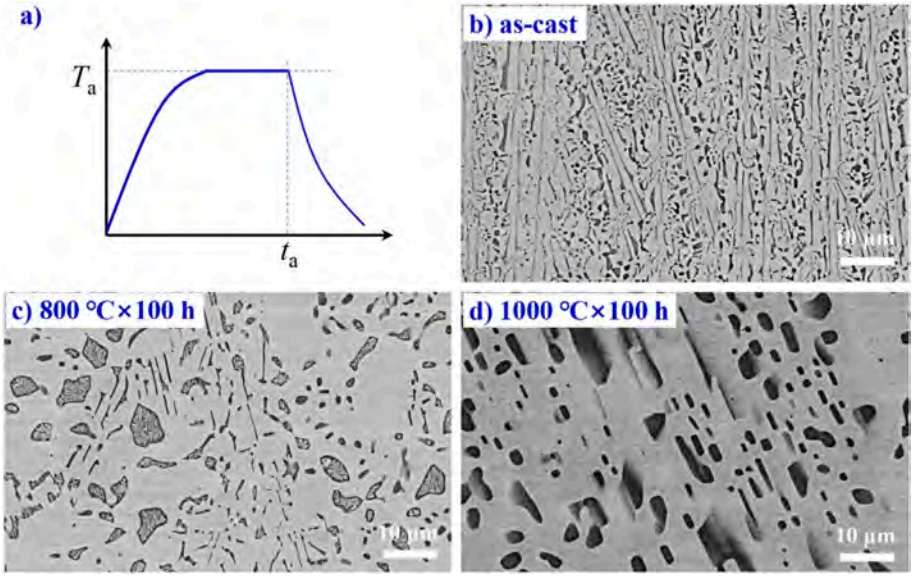

Fig. 9. a) Schematic presentation of isothermal heat treatment; b-d) SEM images of Ni-22Al-7Ti alloy samples with different states.

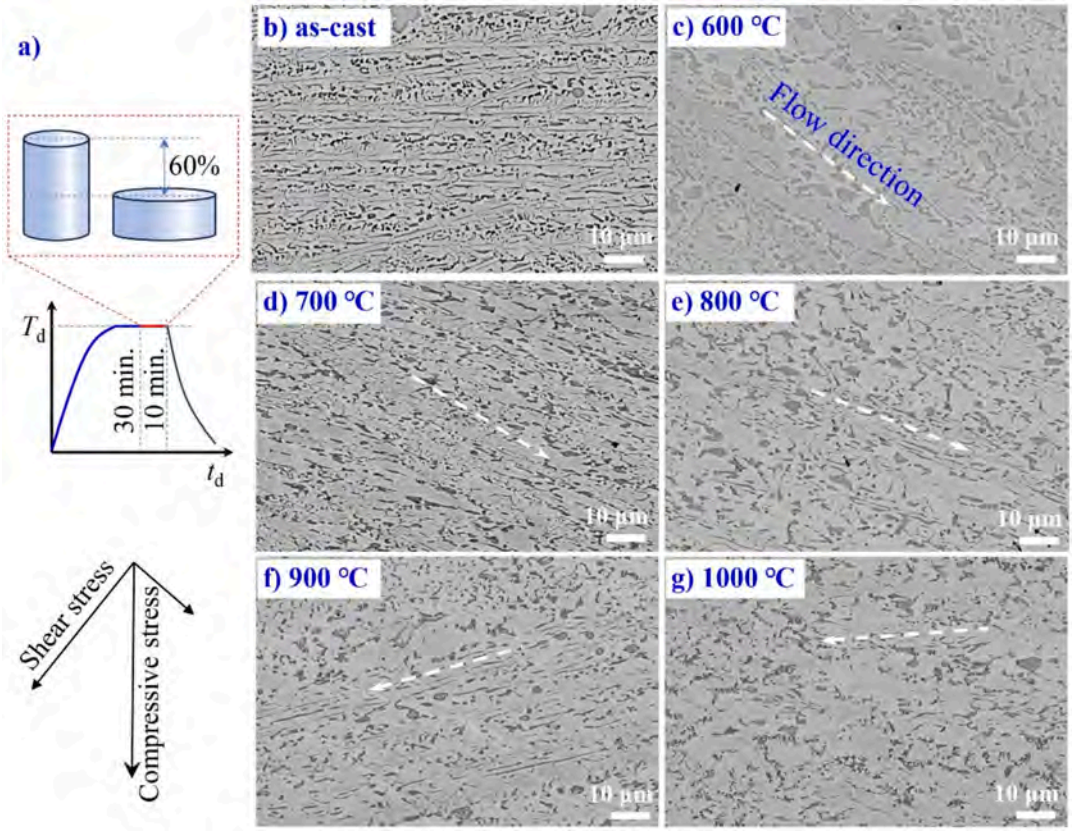

Fig. 10. a) Schematic of the thermal compression process; b-g) SEM images showing the cross-section of the Ni-22Al-7Ti alloy rod in different states after 50% strain.

phases can deform synergistically at RT and HTs. This was also proved by TEM characterization (Fig. 13 a-c) and will be discussed in the following part. The flow direction changes gradually with the increase of the temperature. At 600–700 °C, the flow angle is close to 45°, which is consistent with the high σ_{ys} and σ_{ucs}. It is indicated that additional dislocation slip systems are synchronously activated in the B2 and $L1_2$ phases at HT under high stress [58]. During the thermal processing, typical coarsening and spheroidization behaviors are found in the intermetallic phases, while the volume fraction changes slightly. These results can prove the good thermal processability of dual-intermetallic composite alloys.

It is concluded that the designed Ni-22Al-7Ti alloy not only possesses ultrahigh fracture strength and excellent compressive plasticity at RT, but also exhibits extremely high σ_{ys} close to 1200 MPa at 700 °C. Moreover, the as-cast alloy can maintain structural stability at HT. This alloy is expected to be used as HT structural materials.

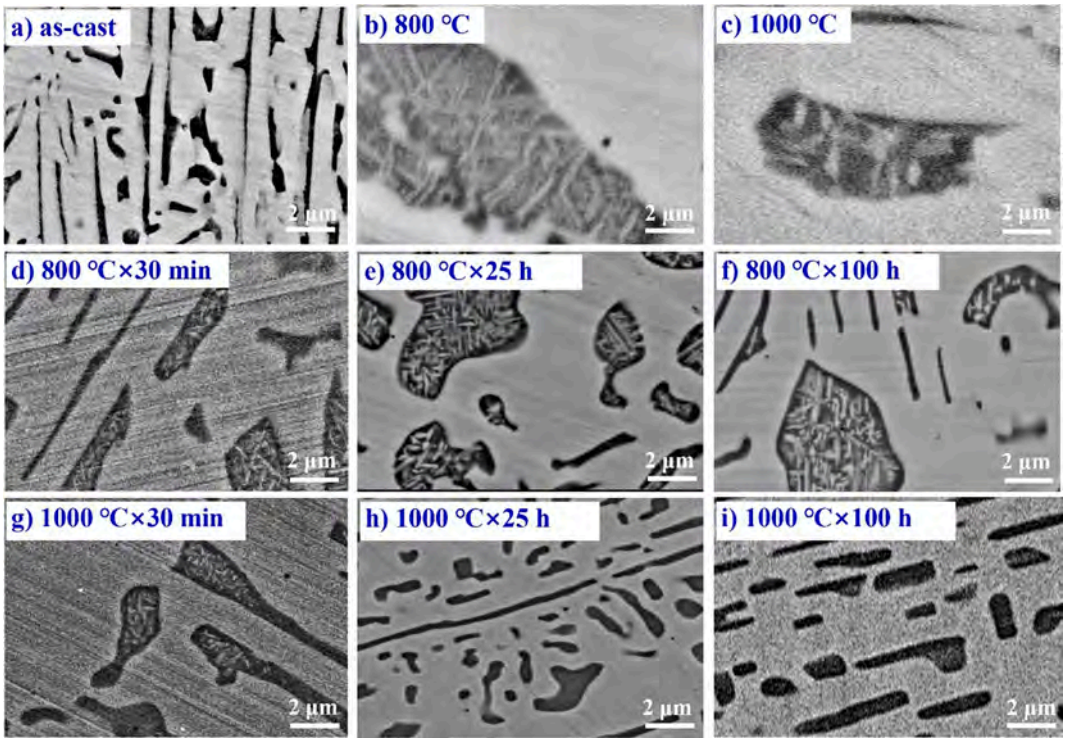

Fig. 11. SEM images focusing on the primary B2 phases in different states to show the secondary $L1_2$ phase precipitation behavior: a) as-cast; b and c) thermally compressed samples; d-g) aged samples.

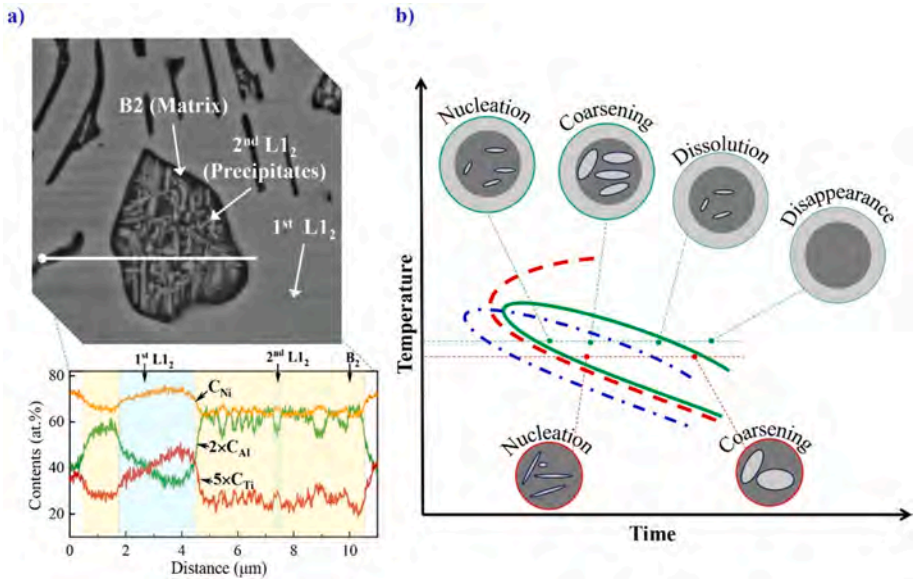

Fig. 12. a) SEM image and line scanning EDS of the 800°C × 100 h heat-treated sample, showing the B2 matrix, primary (1st) $L1_2$ and secondary (2nd) $L1_2$ precipitates; b) TTT curves of the 2nd $L1_2$ phase (in the nose region) in B2 phase, showing microstructure evolution processes of the three phases in the two-fold composite structure: the red one shows the typical nucleation-coarsening process for two phase alloys; the green one shows the nucleation-coarsening-dissolution process of the 2nd $L1_2$ phase in terms of the Oswald ripening mechanism; the blue one shows the acceleration effects of coupled thermal and stress fields.

5. Discussions

For this dual-intermetallic composite alloy with unexpected mechanical property and microstructural stability, there should be some new and interesting mechanisms that are different from the traditional alloys. Here, we focus on the correlation between structure evolution and structure-mechanics.

5.1. Mechanisms of microstructure evolution

Apart from the common grain coarsening and spheroidization, the most interesting evolution in this alloy is the unexpected precipitation behavior. As shown in Fig. 11, a nano-sized acicular second precipitate is found within the B2 phase in the samples after age treatment and thermal processing. It is interesting that the acicular phase is stable in the 800 °C aged sample, while it appears first and then disappears in the

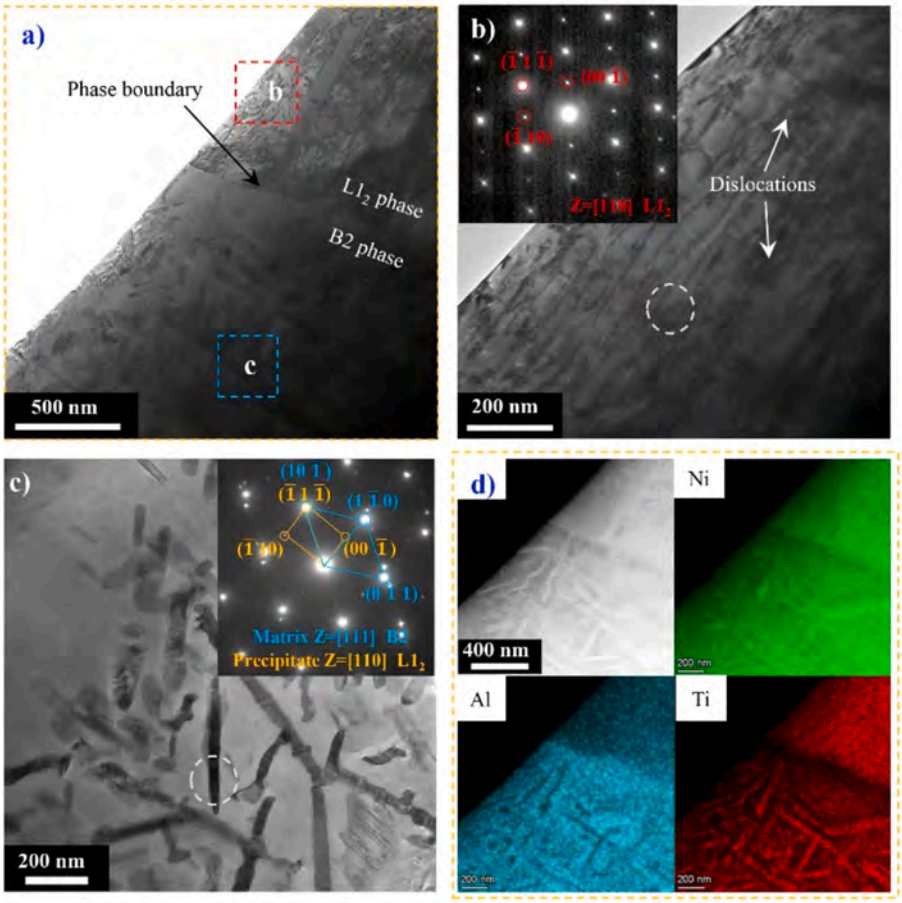

Fig. 13. TEM images of the sample deformed at 800 °C after 20 % compressive strain. a) BF image showing the $L1_2$ and B2 phases after synergistic deformation; b) BF image and SAED pattern showing extensive dislocations in $L1_2$ phase; c) BF image and SAED pattern showing nano-scaled 2nd $L1_2$ particles precipitated in the B2 phase; d) Elemental distributions of the B2 phase, primary and 2nd $L1_2$ phases.

1000 °C aged samples. Compared with the 800 °C × 30 min aged sample, the acicular phase in the thermally compressed sample (the isothermal time is also about 30 min.) exhibits obviously larger size, indicating that the coupled of thermal and force fields can accelerate the coarsening of the acicular phase.

In order to deeply understand the precipitation behaviors of the nano-phase in the B2 phase, an EDS is employed to determine the elemental content of the phases. As shown in Fig. 12 a, the nano-precipitates exhibit high Ni and Ti contents as well as a low Al content, which is similar to the primary $L1_2$-Ni_3 (Al, Ti) phase. Combined with the determination of an XRD pattern, we knew that the secondary precipitate is also the $L1_2$-Ni_3 (Al, Ti) phase (2nd $L1_2$). From the difference between our results and the phase diagram, it is deduced that the precipitation and dissolution of the 2nd $L1_2$ mainly originate from the non-equilibrium solidification induced super-saturation in the B2 phase. When it is heat-treated, the excess Ni and Ti will diffuse from the B2 phase and the 2nd $L1_2$ can form. In the sample heat-treated at a high temperature for a long time, the excess Ni and Ti atoms will diffuse from the B2 phase and lead to an equilibrium phase. In the thermal compression process, the stress can accelerate the diffusion, which will stimulate the 2nd $L1_2$ precipitation and coarsening.

Accordingly, we can propose the microstructure evolution process shown in Fig. 12b. For the as-cast super-saturated alloy, it is understandable that the precipitation of 2nd $L1_2$ from the B2 phase follows a classical nucleation-coarsening process with a common TTT curve. Since the 1st $L1_2$ with a much larger grain size exhibits a lower surface energy than the 2nd $L1_2$, the two-fold composite structure can't be stably coexisted. At HT, the dissolution of the 2nd $L1_2$ will follow the Ostwald Ripening Mechanism [59]. The evolution of the 2nd $L1_2$ will follow the process of nucleation, coarsening, dissolution, and disappearance, in which the B2 phase gives energy for the formation and temporarily stabilizes the 2nd $L1_2$, leading to an improved TTT curve. Moreover, the thermal–mechanical coupling can accelerate the process, resulting in the movement of the TTT curve.

After the dissolution of the 2nd $L1_2$, the sample is composed of B2 and $L1_2$ phase in equilibrium state. The high structural stability at HT of 1000 °C of the dual-intermetallic composite alloy should be ascribed to the following aspects: 1) the intermetallic phases are intrinsically stable owing to the coexistence of metallic and covalent bonds. The B2 and $L1_2$ single-phase alloys are well known for their stable long-range ordered crystalline structures even up to their melting points, which are commonly used in HT fields. 2) Both B2 and the $L1_2$ phases are composed of Ni, Al and Ti elements, their compositions identified in Fig. 5e are closed. The small composition difference will deter the diffusion at HT. This should be additionally benefit for the HT application.

5.2. *Microstructure evolution and mechanical property correlation*

A TEM was employed to further explore the structure and composition of the composite alloy. As shown in Fig. 13a-c, the eutectic phases are confirmed as $L1_2$ and B2 phases, and the nano-particles precipitated in the B2 phase is the 2nd $L1_2$ phase. The primary and 2nd $L1_2$ phase exhibit high Ni and Ti contents as well as a low Al content (Fig. 13d), which is consistent with the SEM-EDS result in 800 °C×100h heat-treated sample (Fig. 12a). Moreover, A large number of dislocations

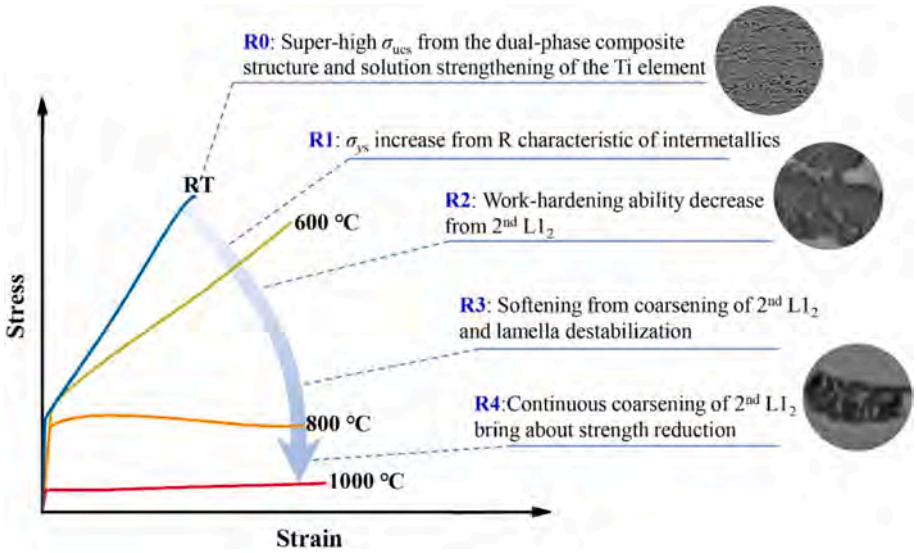

Fig. 14. The schematically illustrated the mechanism of the correlation between phase microstructure and mechanical properties.

can be observed in the $L1_2$ grain, showing the strong deformation ability. In the B2 grain, only a few dislocations are found, which should be attributed to the fine precipitates stimulated recovery and recrystallization. It is known that the formation of new phase always consumes the dislocations stored during deformation. The dense dislocations in the $L1_2$ grain indicates the uniform deformation (Fig. 13b). At HT, the work-hardening ability and strength decrease, which are also owing to the precipitation of the 2nd $L1_2$ from the B2.

In this composite alloy with two intermetallic phases, the correlation between microstructure and mechanical properties at different temperatures should be of a distinct mechanism shown in Fig. 14. At RT, the super-high σ_{ucs} can be explained for two reasons, the one is that the Ni-22Al-7Ti alloy comprising the $L1_2$ and B2 phases deforms synergistically. Yang [33] et al. proposed the corresponding deformation mechanism, plastic deformation initiates in the soft $L1_2$ phase, resulting in internal stress concentrated on the hard B2 phase boundaries. On the other hand, the Ti element brings the solid-solution strengthening effect. The substitution of Ti for the Al atom can result from lattice distortion while stabilizing the phase structure. At medium-temperature, with the increase of temperature, the σ_{ys} exhibit increase–decrease change and the peak value occurring at 700 °C, which is originated from the R characteristic of the intermetallics and more additional dislocation slip systems are synchronously activated in two phases at high temperature under high stress [58]. At HT, the decreased work-hardening ability is owing to the precipitation of the 2nd $L1_2$ from the B2. Moreover, the structure changes from the B2 (hard phase) to the $L1_2$ (soft phase) resulting in the reduced softening-resistance ability. Additionally, the coarsening of the 2nd $L1_2$ and lamella structure destabilization also exacerbates the softening of the alloy. Furthermore, the interface relationship between the 2nd $L1_2$ and matrix can be destroyed under the coupled thermal and stress fields, leading to continuous coarsening of the 2nd $L1_2$ and reduction of σ_{ys}.

6. Conclusions

In this study, we proposed a valid material design strategy for the development of softening resistance and high thermal-stable alloys by constructing the composite dual-intermetallic phases structure. Based on this novel strategy, we successfully designed a series of Ni-Al-Ti system eutectic alloys with $L1_2$-Ni_3Al and B2-NiAl intermetallic. The mechanical properties and microstructural stability of the representative Ni-22Al-7Ti (at. %) alloy were investigated systematically. The following conclusions can be drawn:

1. The Ni-22Al-7Ti eutectic alloy with lamellar composited B2-Ni (Al, Ti) and $L1_2$-Ni_3 (Al, Ti) intermetallic phases is obtained with the assistance of equilibrium phase diagram, CALPHAD and experimental verification. Accordingly, the alloy shows excellent castability under the common casting process due to the composition approaching the eutectic point.
2. This alloy exhibits an ultra-high fracture strength of 3500 MPa and an unexpected fracture strain of 30% under compression test at room temperature, far outperforming their single-phase counterparts. The superior mechanical properties are attributed to the synergetic deformation of the eutectic structure.
3. It is very interesting that this alloy has a much higher σ_{ys} than typical heat-resistance alloys and shows the unusual temperature dependence of the σ_{ys}. The σ_{ys} is increases with increasing temperature, and reaches to a peak value of 1200 MPa at 700 °C. The outstanding mechanical property in the wide temperature range mainly originated from the R characteristic of the $L1_2$-Ni_3 (Al, Ti) intermetallic and Ti alloying stabilizes the phase structure.
4. The dual-phase composite structure is extremely stable at 800 °C and 1000 °C under the coupled thermal and stress fields, which shows great potential for high-temperature structural material applications.

CRediT authorship contribution statement

Mengqi Gao: Writing – original draft, Methodology, Investigation, Formal analysis, Conceptualization. **Donghui Wen:** Writing – review & editing, Supervision, Formal analysis, Conceptualization. **Zhaowen Huang:** Methodology, Formal analysis. **Fengyu Kong:** Resources, Methodology, Investigation. **Junhu Liu:** Methodology, Investigation. **Qiang Li:** Writing – review & editing, Resources, Methodology. **Cong Zhang:** Methodology, Formal analysis. **Chain-Tsuan Liu:** Writing – review & editing, Resources, Conceptualization. **Anding Wang:** Writing – review & editing, Supervision, Resources, Methodology, Conceptualization.

Declaration of competing interest

The authors declare that they have no known competing financial interests or personal relationships that could have appeared to influence the work reported in this paper.

Acknowledgments

This work was supported by National Natural Science Foundation of China (Grant No. 52201175, 52101130, 52271143, 52261033), Guangdong Basic and Applied Basic Research Foundation (Grant No. 2022B1515120027, 2023A1515110130), and Xinjiang Uygur Autonomous Region (Grand No. XJ2023G021).

Data availability

No data was used for the research described in the article.

References

[1] R. Reed, The Superalloys Fundamentals and Applications, Cambridge University Press, Cambridge, 2006.
[2] B. Geddes, H. Leon, X. Huang, Superalloys : Alloying and Performance, Materials Park, Ohio, 2010.
[3] T. Czeppe, S. Wierzbinski, Structure and mechanical properties of NiAl and Ni_3Al-based alloys, Int. J. Mech. Sci. 42 (2000) 1499-1518, https://doi.org/ 10.1016/S0020-7403(99)00087-9.
[4] C.T. Liu, E.P. George, V.K. Sikka, S.C. Deevi, Design of Ni_3Al alloys for structural use, in: N.S. Stoloff, R.H. Jones (Eds.), Processing and Design Issues in High Temperature Materials, the Minerals, Metals & Materials Society, Davos, 1996, pp. 139–157.
[5] Z.H. Huang, Z. Lu, S.S. Jiang, C.Y. Wang, K.F. Zhang, Dynamic recrystallization behavior and texture evolution of NiAl intermetallic during hot deformation, J. Mater. Eng. Perform. 26 (2017) 2377–2387, https://doi.org/10.1007/s11665-017-2594-x.
[6] T. Yang, Y.L. Zhao, J.H. Luan, B. Han, J. Wei, J.J. Kai, C.T. Liu, Nanoparticles-strengthened high-entropy alloys for cryogenic applications showing an exceptional strength-ductility synergy, Scr. Mater. 164 (2019) 30-35, https://doi.org/ 10.1016/j.scriptamat.2019.01.034.
[7] N.S. Stoloff, V.K. Sikka, Physical Metallurgy and processing of Intermetallic Compounds, Boston, Springer, US, MA, 1996.
[8] X. Zhu, Y. He, Q. Feng, N. Wang, C. Ge, Y. Xu, Deformation mechanism of $L1_2$-type multicomponent intermetallics: The generalized stacking fault energy and chemical bonds, Mater. Des. 228 (2023) 111824, https://doi.org/ 10.1016/j.matdes.2023.111824.
[9] C.M. Ward-Close, R. Minor, P.J. Doorbar, Intermetallic-matrix composites-a review, Intermetallics 4 (1996) 217–229, https://doi.org/10.1016/0966-9795(95)00037-2.
[10] J. Chengchang, I. Kiyohito, N. Taiji, Experimental and thermodynamic analysis on phase equilibria of Ni-rich region in Ni-Al-Ti system, Rare Met. 19 (2000) 116–117, https://doi.org/10.1007/s002699900079.
[11] S. C. Duan, X. Shi, M.C. Zhang, B. Li, G. X. Dou, H. J. Guo, J. Guo, Determination of the thermodynamic properties of Ni-Ti, Ni-Al, and Ti-Al, and nickel-rich Ni-Al-Ti melts based on the atom and molecule coexistence theory, J. Mol. Liq. 294 (2019) 111462, https://doi.org/ 10.1016/j.molliq.2019.111462.
[12] T. Yang, Y.L. Zhao, Y. Tong, Z.B. Jiao, J. Wei, J.X. Cai, X.D. Han, D. Chen, A. Hu, J. J. Kai, K. Lu, Y. Liu, C.T. Liu, Multicomponent intermetallic nanoparticles and superb mechanical behaviors of complex alloys, Science 362 (2018) 933, https://doi.org/10.1126/science.aas8815.
[13] T. Yang, B.X. Cao, T.L. Zhang, Y.L. Zhao, W.H. Liu, H.J. Kong, J.H. Luan, J.J. Kai, W. Kuo, C.T. Liu, Chemically complex intermetallic alloys: A new frontier for innovative structural materials, Mater. 52 (2022) 161–174, https://doi.org/10.1016/j.mattod.2021.12.004.
[14] K. Aoki, O. Izumi, Flow stress and work hardening in Ni_3 (Al,Ti) single crystals, Acta Mater. 26 (1978) 1257–1263, https://doi.org/10.1016/0001-6160(78)90010-X.
[15] P.H. Thornton, R.G. Davies, T.L. Johnston, The temperature dependence of the flow stress of the γ′ phase based upon Ni_3Al, Mater. Trans. B. 1 (1970) 207–218, https://doi.org/10.1007/BF02819263.
[16] C.T. Liu, Physical metallurgy and mechanical properties of ductile ordered alloys (Fe Co, Ni)$_3$ V, Metall. Rev. 29 (1984) 168–194, https://doi.org/10.1179/imtr.1984.29.1.168.
[17] I.S. Jeong, J.H. Lee, Single-phase lightweight high-entropy alloys with enhanced mechanical properties, Mater. Des. 227 (2023) 111709, https://doi.org/10.1016/j.matdes.2023.111709.
[18] Z. Wu, H. Bei, G.M. Pharr, E.P. George, Temperature dependence of the mechanical properties of equiatomic solid solution alloys with face-centered cubic crystal structures, Acta Mater. 81 (2014) 428–441, https://doi.org/10.1016/j.actamat.2014.08.026.
[19] I. Voiculescu, V. Geanta, R. Ştefănoiu, A. Rotariu, E. Scutelnicu, M. Pantilimon, D. Mitrică, V. Craciun, New refractory high entropy alloys, IOP Conf. Ser.: Mater. Sci. Eng. 572 (2019) 012024, https://doi.org/10.1088/1757-899X/572/1/012024.
[20] T. Yang, Y.L. Zhao, W.H. Liu, J.H. Zhu, J.J. Kai, C.T. Liu, Ductilizing brittle high-entropy alloys via tailoring valence electron concentrations of precipitates by controlled elemental partitioning, Mater. Res. Lett. 6 (2018) 600–606, https://doi.org/10.1080/21663831.2018.1518276.
[21] Z.M. Li, F. Kormann, B. Grabowski, J. Neugebauer, D. Raabe, Ab initio assisted design of quinary dual-phase high-entropy alloys with transformation-induced plasticity, Acta Mater. 136 (2017) 262–270, https://doi.org/10.1016/j.actamat.2017.07.023.
[22] R.K. Nutor, Q. Cao, R. Wei, Q. Su, G. Du, X. Wang, F. Li, D. Zhang, J.-Z. Jiang, A dual-phase alloy with ultrahigh strength-ductility synergy over a wide temperature range, Sci. Adv. 7 (2021) 4404, https://doi.org/10.1126/sciadv.abi4404.
[23] A.M. Giwa, Z.H. Aitken, P.K. Liaw, Y.W. Zhang, J.R. Greer, Effect of temperature on small-scale deformation of individual face-centered-cubic and body-centered-cubic phases of an $Al_{0.7}$CoCrFeNi high-entropy alloy, Mater. Des. 108611 (2020) 191, https://doi.org/10.1016/j.matdes.2020.108611.
[24] L.C. Hsiung, H.K.D.H. Bhadeshia, Thermodynamically stable β[Ni(Al,Ti)]-β′[Ni_2AlTi]-γ[Ni_3(Al,Ti)] metal-metal composites, Mater. Trans. A. 26 (1995) 1895–1903, https://doi.org/10.1007/BF02670777.
[25] Y. Jiao, L.C. Xu, W.J. Dan, Y.S. Xu, W.G. Zhang, Atomic-scale study of the mechanical properties of dual-phase fcc/bcc crystallites: influences of alloying elements and phase boundaries, J. Mater. 57 (2022) 11111-11131, https://doi.org/ 10.1007/s10853-022-07307-4.
[26] Z. Yang, B. Fu, Z. Ning, X. Bai, H. Yang, Q. Chen, D. Luo, N. Qiu, Y. Wang, Amorphization activated by semicoherent interfaces of FCC/BCC HEA multilayers during deformation, Mater. Des. 225 (2023) 111469, https://doi.org/10.1016/j.matdes.2022.111469.
[27] S.H. Kim, H. Kim, N.J. Kim, Brittle intermetallic compound makes ultrastrong low-density steel with large ductility, Nature. 518 (2015) 77, https://doi.org/ 10.1038/nature14144.
[28] D.D. Zhang, J. Kuang, H. Xue, J.Y. Zhang, G. Liu, J. Sun, A strong and ductile NiCoCr-based medium-entropy alloy strengthened by coherent nanoparticles with superb thermal-stability, J. Mater. Sci. Technol. 132 (2023) 201–212, https://doi.org/10.1016/j.jmst.2022.06.012.
[29] S.B. Haider, E. Heon, M. Neveau, P. Chen, A. Houston, O. Rios, E.A. Lass, Castable eutectic Ni-Ce high temperature alloys strengthened by γ/γ' microstructure, J. Mater. Res. Technol. 28 (2024) 3943–3950, https://doi.org/10.1016/j.jmrt.2023.12.263.
[30] Y. Wang, M. Lu, Z. Wang, J. Liu, L. Xu, Z. Qin, Z. Wang, B. Wang, F. Liu, J. Wang, The learning of the precipitates morphological parameters from the composition of nickel-based superalloys, Mater. Des. 206 (2021) 109747, https://doi.org/10.1016/j.matdes.2021.109747.
[31] X. Chen, J.Q. Qi, Y.W. Sui, Y.Z. He, F.X. Wei, Q.K. Meng, Z. Sun, Effects of aluminum on microstructure and compressive properties of Al-Cr-Fe-Ni eutectic multi-component alloys, Mater. Sci. Eng. A. 681 (2017) 25–31, https://doi.org/j.msea.2016.11.019.
[32] Y. Ma, Q. Wang, X. Zhou, J. Hao, B. Gault, Q. Zhang, C. Dong, T.G. Nieh, A novel soft-magnetic B2-based multiprincipal-element alloy with a uniform distribution of coherent body-centered-cubic nanoprecipitates, Adv. Mater. 33 (2021), https://doi.org/10.1002/adma.202006723 e2006723.
[33] R. Yang, J.A. Leake, R.W. Cahn, Slip transfer from γ′ to β phase in a Ni-Al-Ti alloy, MRS Proc. 288 (1992) 489–494, https://doi.org/10.1557/PROC-288-489.
[34] B. Chanda, G. Potnis, P.P. Jana, J. Das, A review on nano-/ultrafine advanced eutectic alloys, J. Alloys Compd. 827 (2020) 154226, https://doi.org/10.1016/j.jallcom.2020.154226.
[35] A.V. Catalina, P.W. Voorhees, R.K. Huff, A.L. Genau, A model for eutectic growth in multicomponent alloys, Mcwasp Xiv: International Conference on Modelling of Casting, Iop Publishing Ltd, Bristol, Welding and Advanced Solidification Processes, 2015.
[36] P. Shi, R. Li, Y. Li, Y. Wen, Y. Zhong, W. Ren, Z. Shen, T. Zheng, J. Peng, X. Liang, P. Hu, N. Min, Y. Zhang, Y. Ren, P. Liaw, D. Raabe, Y. Wang, Hierarchical crack buffering triples ductility in eutectic herringbone high-entropy alloys, Science. 373 (2021) 912-918, https://doi.org/ 10.1126/science.abf6986.
[37] G. López, S. Sommadossi, W. Gust, E.J. Mittemeijer, P. Zieba, Phase characterization of diffusion soldered Ni/Al/Ni interconnections, Interf. Sci. 10 (2002) 13–19, https://doi.org/10.1023/A:1015172710411.
[38] R. Yang, N. Saunders, J.A. Leake, R.W. Cahn, Equilibria and microstructural evolution in the β/β′/γ′ region of the Ni-Al-Ti system: Modelling and experiment, Acta Metall. Mater. 40 (1992) 1553–1562, https://doi.org/10.1016/0956-7151(92)90098-Y.
[39] P. Willemiin, M. Durand-Charre, The nickel-rich corner of the Ni-Al-Ti system, J. Mater. Sci. 25 (1990) 168–174, https://doi.org/10.1007/BF00544203.
[40] D. Liu, P. Yu, G. Li, P.K. Liaw, R. Liu, High-temperature high-entropy alloys $Al_xCo_{15}Cr_{15}Ni_{70-x}$ based on the Al-Ni binary system, Mater. Sci. Eng. A. 724 (2018) 283-288, https://doi.org/ 10.1016/j.msea.2018.03.058.
[41] H. He, J. Fang, Z. Yang, T. Sun, B. Ma, H. Chen, T. Guo, W. Wang, Y. Shen, M. Wen, Effects of Hf and C on microstructure and mechanical properties of $Re_{0.1}Hf_xTa_{1.6}W_{0.4}(TaC)_y$ refractory medium-entropy alloy, Int. J. Refract. Met. Hard Mater. 121 (2024) 106668, https://doi.org/ /10.1016/j.ijrmhm.2024.106668.
[42] H.T. He, J.X. Fang, J.X. Wang, T. Sun, Z. Yang, B. Ma, H.T. Chen, M. Wen, Carbide-reinforced $Re_{0.1}Hf_{0.25}NbTaW_{0.4}$ refractory high-entropy alloy with excellent room and elevated temperature mechanical properties, Int. J. Refract. Met. Hard Mater. 116 (2023) 106349, https://doi.org/10.1016/j.ijrmhm.2023.106349.
[43] H.T. He, J.X. Fang, Z. Yang, T. Sun, B. Ma, H.T. Chen, T.T. Guo, W.B. Wang, Y.J. Wang, Ductile $Re_{0.1}Ta_{1.9}W_{0.2}C_x$ refractory alloys with excellent elevated-temperature strength, Mater. Sci. Eng. A. 915 (2024) 147217, https://doi.org/10.1016/j.msea.2024.147217.
[44] Y. Koizumi, Y. Ro, S. Nakazawa, H. Harada, NiTi-base intermetallic alloys strengthened by Al substitution, Mater. Sci. Eng. A. 223 (1997) 36–41, https://doi.org/10.1016/S0921-5093(96)10508-6.

[45] X. Jin, Y. Zhou, L. Zhang, X. Du, B. Li, A new pseudo binary strategy to design eutectic high entropy alloys using mixing enthalpy and valence electron concentration, Mater. Des. 143 (2018) 49–55, https://doi.org/10.1016/j.matdes.2018.01.057.
[46] M. Wang, Y. Lu, T. Wang, C. Zhang, Z. Cao, T. Li, P.K. Liaw, A novel bulk eutectic high-entropy alloy with outstanding as-cast specific yield strengths at elevated temperatures, Scr. Mater. 204 (2021) 114132, https://doi.org/10.1016/j.scriptamat.2021.114132.
[47] Y.P. Lu, Y. Dong, S. Guo, L. Jiang, H.J. Kang, T.M. Wang, B. Wen, Z.J. Wang, J. C. Jie, Z.Q. Cao, H.H. Ruan, T.J. Li, A promising new class of high-temperature alloys: eutectic high-entropy alloys, Sci. Rep. 4 (2014) 5, https://doi.org/10.1038/srep06200.
[48] H.P. Wang, C.H. Zheng, P.F. Zou, S. Yang, L. Hu, B. Wei, Density determination and simulation of Inconel 718 alloy at normal and metastable liquid states, J. Mater. Sci. Technol. 34 (2017) 22–25, https://doi.org/10.1016/j.jmst.2017.10.014.
[49] A.E. Staton-Bevan, R.D. Rawlings, The deformation behaviour of single crystal Ni_3(Al, Ti), Phys. Stat. Sol. (a) 29 (1975) 613–622, https://doi.org/10.1002/pssa.2210290232.
[50] X. Ye, J. Xiong, X. Wu, C. Liu, D. Xu, W. Zhang, D. Fang, B. Li, A new infinite solid solution strategy to design eutectic high entropy alloys with B2 and BCC structure, Scr. Mater. 199 (2021) 113886, https://doi.org/10.1016/j.scriptamat.2021.113886.
[51] Y. Dong, Y. Lu, J.J. Zhang, T.J. Li, Microstructure and Properties of Multi-Component $Al_xCoCrFeNiTi_{0.5}$ High-Entropy Alloys, Mater. Sci. Forum. 745-746 (2013) 775 - 780, https://doi.org/10.4028/www.scientific.net/MSF.745-746.775.
[52] X. Xian, Z.H. Zhong, L.J. Lin, Z.X. Zhu, C. Chen, Y.C. Wu, Tailoring strength and ductility of high-entropy CrMnFeCoNi alloy by adding Al, Rare Met. 41 (2022) 1015–1021, https://doi.org/10.1007/s12598-018-1161-4.
[53] K. Yao, L. Liu, J. Ren, Y. Guo, Y. Liu, Y. Cao, R. Feng, F. Wu, J. Qi, J. Luo, P.K. Liaw, W. Chen, High-entropy intermetallic compound with ultra-high strength and thermal stability, Scr. Mater. 194 (2021) 113674, https://doi.org/10.1016/j.scriptamat.2020.113674.
[54] C.S. Han, C.H. Bae, J.H. Lee, Characteristic of microstructure and mechanical properties in Ni-Al-Ti alloy system, Metals Mater. Int. 15 (2009) 891–895, https://doi.org/10.1007/s12540-009-0891-0.
[55] L.H. Mills, M.G. Emigh, C.H. Frey, N.R. Philips, S.P. Murray, J. Shin, D.S. Gianola, T.M. Pollock, Temperature-dependent tensile behavior of the HfNbTaTiZr multi-principal element alloy, Acta Mater. 245 (2023) 118618, https://doi.org/10.1016/j.actamat.2022.118618.
[56] M. Wang, Y. Lu, J. Lan, T. Wang, C. Zhang, Z. Cao, T. Li, P.K. Liaw, Lightweight, ultrastrong and high thermal-stable eutectic high-entropy alloys for elevated-temperature applications, Acta Mater. 248 (2023) 118806, https://doi.org/10.1016/j.actamat.2023.118806.
[57] Y. Zhou, X. Jin, L. Zhang, X. Du, B. Li, A hierarchical nanostructured $Fe_{34}Cr_{34}Ni_{14}Al_{14}Co_4$ high-entropy alloy with good compressive mechanical properties, Mater. Sci. Eng. A. 716 (2018) 235–239, https://doi.org/10.1016/j.msea.2018.01.034.
[58] D. Caillard, J.L. Martin, Thermally Activated Mechanisms in Crystal Plasticity, Pergamon, Amsterdam; Boston, 2003.
[59] T. Maebashi, M. Doi, Coarsening behaviours of coherent γ' and γ precipitates in elastically constrained Ni-Al-Ti alloys, Mater. Sci. Eng. A. 373 (2004) 72–79, https://doi.org/10.1016/j.msea.2003.12.064.